

DOI: 10.1002/adem.201200247

Wetting Properties of Steel Surfaces Modified by Laser Interference Metallurgy**

By Brice Raillard,* Justine Rémond, Esteban Ramos-Moore, Nicolas Souza, Carsten Gachot and Frank Mücklich

The wetting properties of 100Cr6 bearing steel surfaces modified using laser interference metallurgy (LIMET) are analyzed. The steel surfaces are structured with line-like patterns with line-spacing. The topography of the ridged surface is analyzed by means of white light interferometry and scanning electron microscopy and surface chemistry of the different topographic regions by Raman spectroscopy. Contact angle (CA) measurements are performed on modified and non-irradiated surfaces, using bi-distilled water and FVA2 industrial oil. The angles are measured parallel and perpendicular to the line-pattern orientation. The topographical analysis shows steep line-pattern produced by laser. Raman analysis indicates that the laser irradiation does not significantly change the chemical species of the modified surfaces. The CA measurements elucidates that the parallel orientation provides a better wetting of the surface, because the laser line-pattern acts as capillary flow channels, whereas the perpendicular orientation imposes energy barrier thus preventing wetting. As expected, the wetting coverage is more effective for larger than for smaller periodic structures, due to the larger area of flat contact. These novel results highlight the relevant use of LIMET to tailor the wetting properties of steel surfaces.

The tailoring of wettability is a worldwide exciting topic, which represents significant investments for the pharmaceutical, food, petroleum, and automotive industries.^[1–4] Depending on the application domain, two options are available to control and tailor the wetting. First, the wetting properties of a fluid can be changed by adding surfactants^[5] or particles.^[6] For example, Tanvir and Qiao^[7] found that high concentrations of Al and Al₂O₃ nanoparticles increased the surface tension of liquid ethanol and fuels. Second, the surface modification also allows for the control of the wetting

properties. Most of the current functional systems that are based in liquid–solid interfaces are inspired by nature,^[8–11] and required the modification of the surface properties. Among others, the sharkskin can be mentioned being efficient in reducing drag and which was already industrially adapted as body swimsuits.^[12] In particular, the laser interference metallurgy (LIMET) technique allows for regular and periodic patterns on the micrometer scale.^[13] In the case of bulk metallic samples,^[14] or silicon,^[15] the laser structuring is governed by the Marangoni convection, which represents a thermocapillary flow of a fluid. Due to the laser irradiation, the molten metal flows from low to high surface tension regions.^[16,17] Through this technique, fundamental material properties such as wear resistance,^[18,19] electric properties,^[20] and wetting^[21,22] can be modified. Gachot *et al.*^[22] studied the effect of laser structuring on the hydrophobic behavior of polyimide and gold thin films. They observed that the laser patterns induced the formation of a composite surface according to the model of Cassie–Baxter increasing the contact angles (CA). Hans *et al.*^[21] also tuned the wettability of polyimide and titanium surfaces by laser interference structuring. They found that less relevant chemical modification was detected after laser irradiation and affirmed that the wetting behavior was mainly governed by the topography and geometrical parameters (periodicity and depth) of the samples.

[*] B. Raillard, J. Rémond, Dr. E. Ramos-Moore, N. Souza, C. Gachot, Prof. F. Mücklich
Campus D3.3 Chair of Functional Materials
Saarland University, 66123 Saarbrücken, Germany
E-mail: b.raillard@mx.uni-saarland.de

Dr. E. Ramos-Moore
Facultad de Física, Pontificia Universidad Católica de Chile
Santiago 7820436, Chile

[**] The authors would gratefully acknowledge the European Union through the project AME-Lab (European Regional Development Fund C/4-EFRE-13/2009/Br), the Deutscher Akademischer Austausch Dienst (DAAD) and Comisión Nacional de Investigación Científica y Tecnológica (CONICYT-Chile) for their contributions and Michael Hans and Dr. Flavio Soldera for their corrections and suggestions.

In the present work, we used the LIMET technique in order to study the wetting properties of a typical bearing steel 100Cr6 depending on the geometrical parameters of the laser structure. The hydrophobic and oleophilic behavior of bulk samples were controlled by functionalizing their surfaces. Distilled water and FVA2 oil were used to study this behavior. The FVA2 oil and the 100Cr6 steel were chosen because of their industrial applications. White light interferometry (WLI) and scanning electron microscopy (SEM) were used to study the topography of the modified surfaces. The chemical composition was studied by Raman spectroscopy and the CA was measured according to the sessile drop method. Our novel results highlight the control of the wettability on steel surfaces, which can benefit self-cleaning applications and lubrications.

1. Experimental

All the samples were prepared by grinding and polishing methods. The LIMET technique was performed as described in a previous work.^[13] The samples were irradiated using a high-energy pulsed Nd:YAG laser working at a wavelength 355 nm with a pulse duration of 10 ns and a repetition rate of 10 Hz. The primary beam was directed through an attenuator, a square-shaped mask and a lens with a focal length of 2 m. The beam was divided using a beam splitter and interfered at the surface of the sample in order to create line-like patterns with controlled periodicity.

The topography of the samples was analyzed using a WLI provided by Zygo (New View 7300) and a SEM (FEI Strata DB 235).

Raman spectroscopy was performed with a LabRAM ARAMIS instrument from HORIBA using a 532 nm laser beam without a filter. The Raman microscope uses a back-scattering geometry, where the incident beam is linearly polarized and the spectral detection unpolarized. The slit and hole size were 100 and 1000 μm , respectively. The objective lenses used in the microscope were 100 \times to minimize the laser spot size. In order to obtain representative and reliable Raman information, the analysis was repeated five times for each configuration at different positions.

The CA and interfacial tension (IFT) measurements were performed with a standard drop shape analyzer (Krüss DSA 100). CA experiments were conducted in static and dynamic modes for distilled water and FVA2 oil, respectively. The values of CA were estimated by calculating the average of the CA measured at both sides of the drop profile. Figure 1 schematically represents the CA measurement in the case of the parallel (a) and perpendicular (b) structure orientation. The parallel (a) and perpendicular (b) configurations correspond to the relative orientation between the propagation direction of the fluid and the pattern lines. Room temperature ($\approx 20 \pm 2^\circ\text{C}$) and relative humidity ($\approx 50 \pm 5\%$) were stable and constant during the experiments. The water and oil drop volumes were chosen between 6 and 7 μl . Before the drop deposition, the samples were all ultrasonically cleaned in cyclohexane, acetone, and ethanol. Once the droplet was

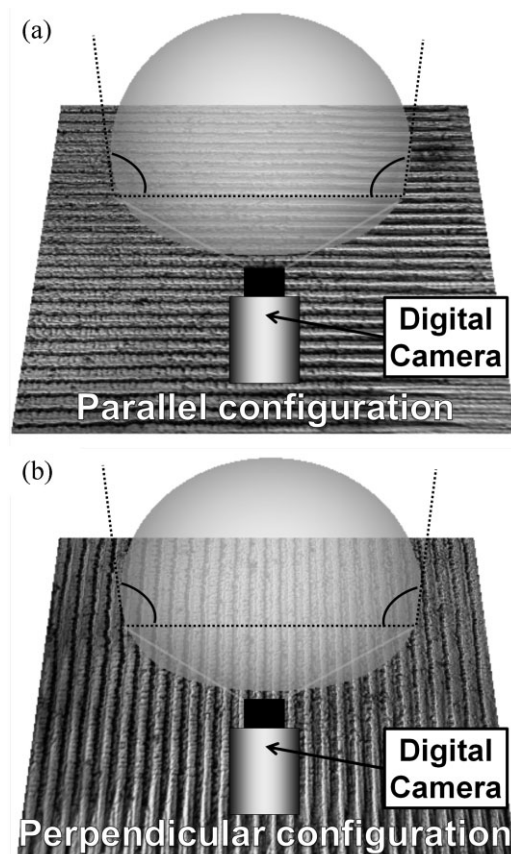


Fig. 1. Schematic representation of the CA measurement in the case of the parallel (a) and perpendicular (b) structure orientation. The values of CA were estimated by calculating the average of the CA on the both sides of the drop profile.

deposited on the sample, videos of the drop propagation were recorded. In both cases (distilled water and oil), the CA was calculated for each second within an interval of 6 s. The measurement duration was decided after experimental considerations: it could be observed that the water droplets were in a steady state after 6 s and it was almost impossible to determine the drop-profile of the oil after 6 s. Indeed, due to the spreading of the oil on the surface, the software was not able to detect the profile of the droplet and then no CA measurement could be achieved. The IFT of FVA 2 oil was estimated: $\text{IFT} = 30.01 \text{ mN m}^{-1}$. Each measurement (CA and IFT) was repeated at least six times in order to obtain statistic representative results, in which errors lower than 5° were registered. It is important to note that the water and oil measurements were performed on the same samples (i.e. exactly the same topography) after cleaning the samples. In order to study the effects of the structure orientation, the CAs were measured for the parallel and perpendicular configurations.

2. Results

2.1. Topographical Analysis

A three-dimensional WLI picture presented in Figure 2 shows the sample surface before the laser patterning. It is worth to note that the metallographic preparation resulted in a flat surface with no preferential orientation, no significant

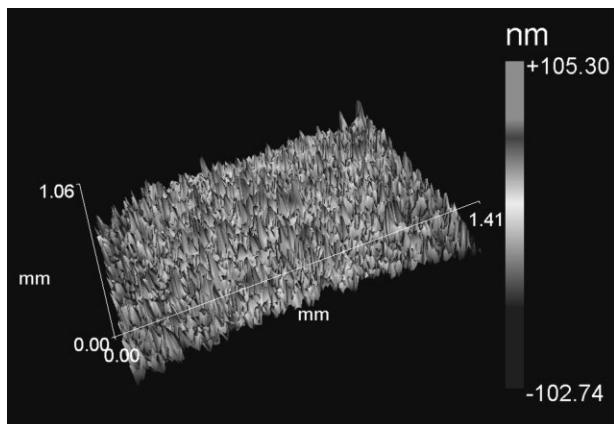


Fig. 2. WLI picture of the grinded and polished steel surfaces prior to LIMET modification. The metallographic preparation resulted in a flat surface with a roughness of 50 nm (R_q).

topographic artefacts, and around 50 nm (root-mean-square roughness (R_q)).

In order to study the effects of the pattern periodicity on the wetting behavior, several patterns with seven different periodicities were fabricated with fluence about 2 J cm^{-2} . The irradiated area of each sample was approximately 1 cm^2 and composed of several adjacent spots of 3 mm^2 . The laser-structured surfaces presented an averaged R_q value of around 580 nm. Figure 3 shows SEM images and depth profiles of the patterns produced on the flat surfaces after LIMET modification using 3.5, 13, and $22 \mu\text{m}$ of period.

The tallest topographic structures (peaks) of each sample were found to have similar height ($\approx 1 \mu\text{m}$) related to the

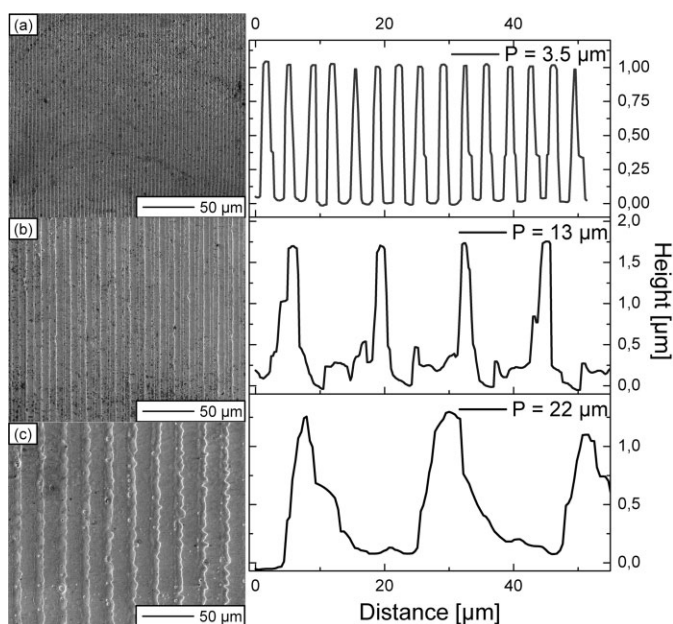


Fig. 3. SEM pictures (left) and WLI depth profiles (right) of the laser line patterns with 3.5 (a), 13 (b), and $22 \mu\text{m}$ (c) periodicities (P). The $3.5 \mu\text{m}$ profile is very regular; the $13 \mu\text{m}$ presents numerous irregularities and a “shallow” peaks. They both have rough patterns. The $22 \mu\text{m}$ structure is more regular and provides the lowest slope of all the patterns.

Table 1. Geometrical parameters of the LIMET structures used for the CA measurements.

Period [μm]	3.5	5	7.5	10	13	15.5	22
Slope	0.83	0.81	0.36	0.35	0.36	0.3	0.11

The height was kept constant around $1 \mu\text{m}$ for all the structured samples.

lowest topographical regions (valleys) independent of the periodicity. The slope of the structures was measured as the distance from the highest point of the peak to the valleys and divided by the corresponding horizontal distance. The periodicity and slopes of the different patterns are resumed in Table 1. As presented in the SEM pictures and WLI depth profiles (Figure 3), the pattern with 3.5 period is very regular in height and width. The peak pattern is rough and presents the highest slope. The $13 \mu\text{m}$ periodicity pattern shows irregular structures that present two distinct parts: a small and a big peak (Figure 3b). Their height and width vary along the line-patterns, and also present topographical “ramifications” or “bridges” between them. The $22 \mu\text{m}$ sample is homogeneous, with only one peak induced by the laser irradiation, and the line structure provides the lowest slope of all the patterns (Table 1).

2.2. Chemical Analysis: Raman Spectroscopy

Raman analysis was performed on the unstructured and irradiated samples in order to observe if the patterned laser surfaces were chemically altered and if the surface chemistry could have a role regarding the wetting behavior. The measurements were performed only on the $22 \mu\text{m}$ period sample because the laser spot size ($\approx 5 \mu\text{m}$ at full width at half maximum) was not small enough to distinguish between peaks and valleys for the samples with lower periodicity. The information depth was around $1 \mu\text{m}$ due to the confocality of the equipment and the optical oculars used ($100\times$). As showed in Figure 4, the Raman-laser spot was focused on the maximum (peak) and minimum (valley) positions of the pattern structure, which correspond to the locations where the pattern irradiation was minimum and maximum, respectively.

As showed in the spectrum of Figure 4, the same Raman modes were found in the reference, peaks and valleys. The low-frequency peak located at $\approx 300 \text{ cm}^{-1}$ corresponds to vibrations observed in Fe_2O_3 , whereas the peaks located at ≈ 530 and $\approx 660 \text{ cm}^{-1}$ have been observed in Raman spectra of FeO , Fe_3O_4 , and Fe_2O_3 .^[23,24] Moreover, the peak located at $\approx 810 \text{ cm}^{-1}$ was assigned to chromium oxide species, since Cr–O stretching vibrations located around the same frequency have been observed in compounds containing chromium oxide.^[25–27] Although the chemical species found in the different topographical events are the same, it is worth to note that the increase of the intensity of the peaks located at ≈ 530 and $\approx 660 \text{ cm}^{-1}$ indicates that the abundance of iron oxides is slightly higher in the peaks than in the valleys and unstructured zones.

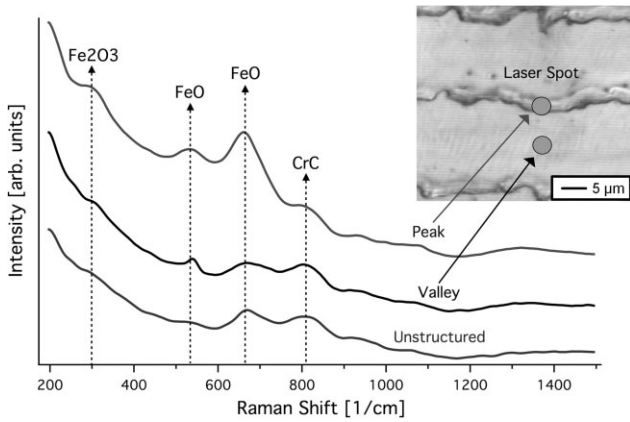


Fig. 4. Raman spectra of the unstructured, valley, and peak zones performed onto 22 μm period structured sample. The inset shows the Raman laser spot size where the spectra were measured using a 100 \times ocular. The abundance of iron oxides is higher in the peaks than in the valleys and unstructured zones.

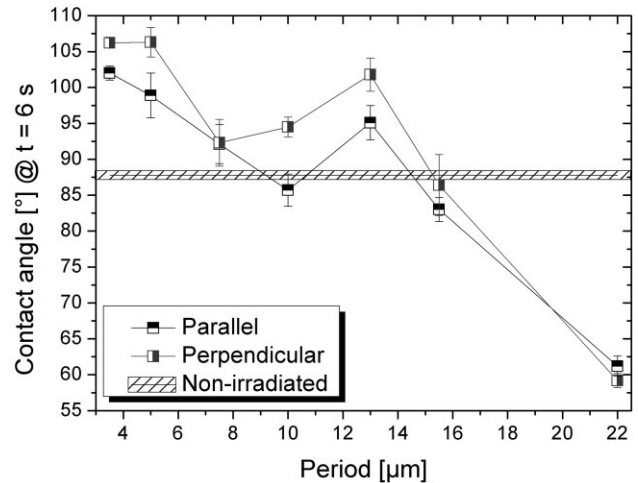


Fig. 6. CA of the water droplets (at 6 s) as a function of the structure periodicity. The structure orientation does not have a significant effect on the hydrophobic behavior while the CA decreases as the period increases.

2.3. Wetting Analysis: Distilled Water

The temporal evolution of the CA of a distilled water droplet onto the non-irradiated and structured surface was measured as a function of the pattern orientation and periodicity. The non-irradiated surface showed a decrease of the CA from 99.2° to 87.8° at six seconds (Figure 5a and b). As observed in Figure 5c and d, the perpendicular line patterns induce the smallest CA at 6 s (59.2°) and provide the most stabilized wetting configuration, due to the small change in the CA at 6 s (61.4–59.2°).

The effect of the pattern periodicity and orientation on the CA is presented in Figure 6. The behavior of the CA measured at 6 s on the parallel and perpendicular patterns show a similar tendency as the period of the laser pattern increases. Independent of the structuring direction, the laser patterns with periods lower than 16 μm present a hydrophobic behavior (CA > 90°). Independent on the periodicity of the laser pattern, the CA measured in the parallel configuration is always lower or similar than the perpendicular orientation. The patterned structures with 22 μm line spacing always present hydrophilic behavior in opposition to the non-irradiated surface, which present hydrophobic–hydrophilic transition.

Three distinct zones can be distinguished in the CA curves: the small (3.5–5 μm), middle (7.5–13.5 μm), and large (15.5–22 μm) periods. The highest CA was 106.3° and was measured in the small period patterns. The CA has a local maximum at 13.5 μm of period, showing a value of 101.8° and 95.1° for perpendicular and parallel orientations, respectively. It is worth to mention that the structures with 22 μm provide a significant smaller CA than the patterns with lower periodicity.

2.4. Wetting Analysis: FVA2 Oil

The CA measurements using FVA2 oil droplets on the surface of non-irradiated and laser structured samples are shown in Figure 7. A reduction of 82% of the CA is observed after the stabilization of the drop on the non-irradiated surface. The parallel orientation with 22 μm period leads to the smallest CA compared to the perpendicular orientation and the non-irradiated state.

In Figure 8, the CA of a FVA2 oil droplet at 6 s is plotted against the patterns periodicity. Although the parallel and perpendicular structured surfaces show a similar tendency as a function of the patterns periodicity, a significant difference of CA between different orientations is observed. For small

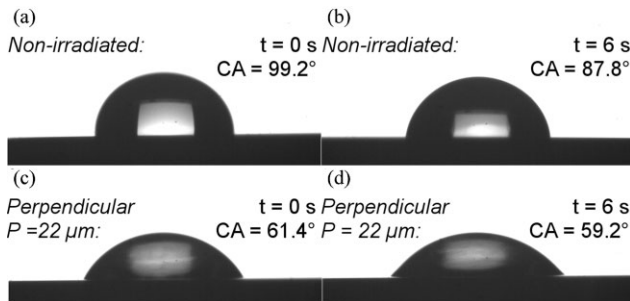


Fig. 5. Temporal evolution of CA measurements using water droplets on non-irradiated (a and b) and laser structured surfaces (c and d). On the unstructured surfaces, a reduction from 99.2° (a) to 87.8° (b) regime is observed at 6 s. The perpendicular structure with 22 μm period has a hydrophilic behavior and tends also to minimize the CA.

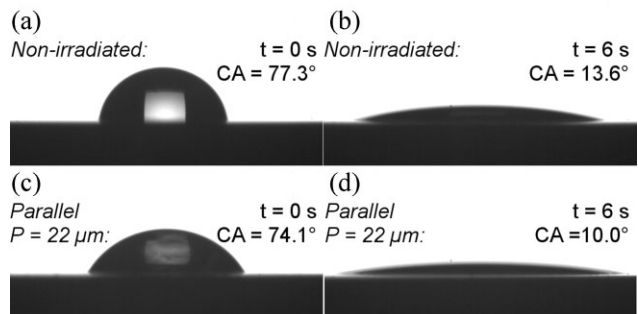


Fig. 7. Temporal evolution of CA measurements using FVA2 oil droplet on non-irradiated (a and b) and 22 μm period parallel structured surfaces (c and d). Both surfaces show oleophilic behavior and the wetting of the non-irradiated surface leads to 82% of reduction in the CA value.

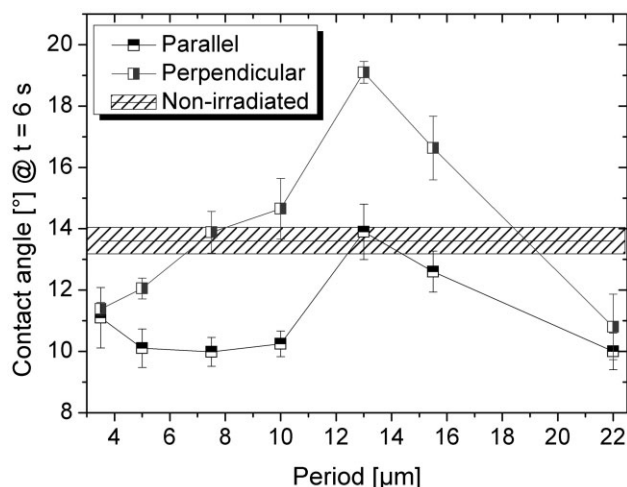


Fig. 8. CA of the FVA2 oil droplets (at 6 s) as a function of the structure periodicity. The structure orientation has a significant effect on wetting behavior. The parallel line pattern provides always a lower CA compared to the perpendicular orientation.

patterns periodicity, the perpendicular orientation shows an increase of the CA, while in the parallel orientation the CA stays stable. Independently on the orientation, a maximum value of the CA is reached for patterns with 13 μm period. The perpendicular line-pattern provides always a similar or higher CA compared to the parallel line orientation. The perpendicular pattern configurations with periods of 10, 13, and 15.5 μm have a CA higher than the unstructured state. Moreover, independently of the period, the parallel structure always provides the smallest CA except for the 13 μm period, which is similar as the unstructured surface.

3. Discussion

Raman spectroscopy analyses performed on the 22 μm samples revealed that the same species were detected in the non-irradiated, structured-maxima (laser-minima) and structured-minima (laser-maxima) regions. Thus, the chemical compositions of the peak/liquid and valley/liquid interfaces are similar. The high concentration of oxides and carbides in the peak regions can be explained by the formation of the laser line structures. This phenomenon is governed by the Marangoni convection, which is explained as follows. By interacting with the metallic surface, the laser beam induces molten material, which is transferred to the “hottest” region and then solidifies in the “coldest” region. Lu *et al.*^[15] used direct laser patterning method in order to structure silicon samples. The Gaussian profile of the laser intensity distribution induced a Marangoni effect in the molten area. Two effects were observed, a thermocapillary effect, which drives the matter from the hot center to the border of the irradiated zone, and a chemicapillary effect that moves the material towards the center. In this work, the laser irradiation was not performed under controlled gas atmosphere but under atmospheric conditions (about $25 \pm 2^\circ\text{C}$ and $50 \pm 5\%$ relative humidity). The molten metal is highly reactive and the oxygen is strongly adsorbed at the surface.^[28,29] For this

reason, we consider our structured samples as chemically homogeneous. Thus, the control of the topography is the key parameter to study the wetting phenomena. Considering that the behavior of a perfectly flat surface is hydrophilic (Figure 5b), the generation of roughness by laser texturing (R_q non-irradiated ≈ 50 nm, R_q laser-irradiated ≈ 580 nm) should lead to a more hydrophilic behavior, according to the model of Wenzel.^[30] However, this assumption is not completely valid for all our structures and the wetting behavior shows to be dependent on the laser periodicity. The Cassie–Baxter model explains the wetting behavior of rough surfaces,^[31] by assuming that the droplet deposited on a rough surface cannot completely wet the surface and leads to the formation of composite surfaces. The composite air-solid surfaces are the results of a non-complete wetting, which leads to the superhydrophobic behavior of micro-^[32] and nano-pillars.^[33] The hydrophobic behavior observed for almost all the laser-irradiated samples may be explained by this hypothesis. Nevertheless, differential interference contrast (DIC) experiments were performed on the wet surfaces and no difference in contrast between the peaks and valleys could be observed. Thus, we conclude that there is no composite surface and that the Cassie–Baxter model does not explain our results.

In contrast to water, the wetting behavior of the FVA2 oil presents a significant dependence of the pattern-orientation. De Gennes, based on the work of Mason^[34] and Cox,^[35] proposed to explain the anisotropy showed by the periodical line-patterns in “Wetting: statics and dynamics”.^[36] He affirmed that in the case of parallel orientation (triple-line perpendicular to the grooves), the fluid would be free to flow inside the groove acting as a capillary channel. This effect was previously observed by Shuttleworth^[37] and Oliver *et al.*^[38] In the case of perpendicular orientation (triple line parallel to the grooves), the droplet is pinned by the grooves, acting as a physical barrier. De Gennes proposed that the overlapping of these energy barriers^[39] is not an “overall jump” of the line but a jump in a single point. After having passed these barriers, the liquid flows inside the grooves. These phenomena justify our observations that the parallel orientation provides a better wetting of the surface because the laser line pattern act as capillary flow channel, while the perpendicular orientation requests more energy to cover the same distance.

The CA of the water droplet on the structured surfaces shows a strong dependency on the pattern periodicity (Figure 8). This phenomenon is correlated with the “effect of the edge”^[40] as found by Oliver *et al.* after measuring the wetting behavior of a droplet on triangle and sinusoidal profiles.^[38] The configurations of 13 and 15.5 μm of period showed higher CA for both perpendicular and parallel orientations. In Figure 3, we clearly observed that the 13 μm patterns present irregularities comparing to the other structures. Even if these topographical faults are smaller than the regular peaks (around 0.5 μm), they increase the number of energy barriers and prevent wetting. Moreover, the heterogeneities in the 13 μm patterns act as a reservoir by retaining oil in all the topographical “cavities and ramifica-

tions" leading to the CA maxima observed in both parallel and perpendicular configurations.

4. Conclusions

We demonstrated that the wetting behavior of 100Cr6 industrial steel surfaces can be tailored by designing precise interference patterns using nanosecond-laser radiation. Raman spectroscopy showed that the chemical species of the laser irradiated and non-irradiated surfaces are similar. A difference in iron oxides concentrations was found depending on the laser intensity distribution due to the Marangoni convection phenomenon. Depending on the pattern orientation and periodicity, the surface modification can lead to hydrophobic and/or hydrophilic behavior. The parallel orientation provides a better wetting of the surface because the laser line-patterns act as capillary flow channels, while the perpendicular orientation imposes energy barriers that prevent wetting. The wetting coverage is more effective for large than for small period structures. This effect leads to tailor the hydrophobic (small periods) or hydrophilic (large periods) behavior, depending on the kind of liquid to be used. Similar wetting effects occur for oil after laser structuring, but no transition from oleophilic to oleophobic was observed. The hydrophobic behavior could be benefit for self-cleaning applications and the olephilic behavior for controlling the lubrication phenomena on the 100Cr6 surfaces.

Received: July 25, 2012

Final Version: October 12, 2012

Published online: November 21, 2012

- [1] D. Zhang, J. H. Flory, S. Panmai, U. Batra, M. J. Kaufman, *Colloids Surf. A: Physicochem. Eng. Aspects* **2002**, 206, 547.
- [2] W. Y. Choi, H. J. Park, D. J. Ahn, J. Lee, C. Y. Lee, *J. Food Sci.* **2002**, 67, 2668.
- [3] I. G. Hwang, K. Choi, J. Kim, C. L. Myung, S. Park, *Proc. Inst. Mech. Eng. [D]* **2012**, 226, 112.
- [4] T. Morimoto, Y. Sanada, H. Tomonaga, *Thin Solid Films* **2001**, 392, 214.
- [5] M. J. Rosen, J. T. Kunjappu, in *Surfactants and Interfacial Phenomena*, 4th Ed., John Wiley & Sons, Hoboken, New Jersey **2012**.
- [6] S. Vafaei, A. Purkayastha, A. Jain, G. Ramanath, T. Borca-Tasciuc, *Nanotechnology* **2009**, 20, 185702.
- [7] S. Tanvir, L. Qiao, *Nanoscale Res. Lett.* **2012**, 7, 226.
- [8] E. A. Favret, in *Functional Properties of Bio-Inspired Surfaces: Characterization and Technological Applications*, World Scientific Pub Co. Inc., Singapore **2009**.
- [9] Z. Guo, W. Liu, B.-L. Su, *J. Colloid Interface Sci.* **2011**, 353, 335.
- [10] K. Koch, B. Bhushan, W. Barthlott, *Soft Matter* **2008**, 4, 1943.
- [11] Z. X. Jiang, L. Geng, Y. D. Huang, S. A. Guan, W. Dong, Z. Y. Ma, *J. Colloid Interface Sci.* **354**, 866.
- [12] B. Bhushan, *Philos. Trans. R Soc. A: Math. Phys. Eng. Sci.* **2009**, 367, 1445.
- [13] F. Mücklich, A. Lasagni, C. Daniel, *Int. J. Mater. Res.* **2006**, 97, 1337.
- [14] M. D'Alessandria, A. Lasagni, F. Mücklich, *Appl. Surf. Sci.* **2008**, 255, 3210.
- [15] Y. Lu, S. Theppakuttai, S. C. Chen, *Appl. Phys. Lett.* **2003**, 82, 4143.
- [16] J. M. Drezet, S. Pellerin, C. Bezençon, S. Mokadem, "Modelling the Marangoni convection in laser heat treatment", presented at *Journal De Physique. IV: JP*, 2004.
- [17] A. Blatter, in *Laser-Beam Interactions With Materials: Physical Principles and Applications*, Vol. 2, Springer Verlag, Berlin **1995**.
- [18] B. Raillard, C. Gachot, M. Hans, P. Leibenguth, F. Mücklich, *Proc. Inst. Mech. Eng. [J]* **2012**, 226, 541.
- [19] R. Catrin, T. Gries, B. Raillard, F. Mücklich, S. Migot, D. Horwat, *J. Mater. Res.* **2012**, 1, 1.
- [20] R. Catrin, D. Horwat, J. F. Pierson, S. Migot, Y. Hu, F. Mücklich, *Appl. Surf. Sci.* **257**, 5223.
- [21] M. Hans, C. Gachot, F. Müller, F. Mücklich, *Adv. Eng. Mater.* **2009**, 11, 795.
- [22] C. Gachot, M. Hans, R. Catrin, U. Schmid, F. Mücklich, *Proc. SPIE* **2009**, 7362, 73620U-1.
- [23] R. L. Farrow, R. E. Benner, A. S. Nagelberg, P. L. Mattern, *Thin Solid Films* **1980**, 73, 353.
- [24] R. K. S. Raman, B. Gleeson, J. Young D Mater. Sci. Technol. **2011**, 14, 373.
- [25] B. M. Weckhuysen, I. E. Wachs, *J. Phys. Chem. B* **1997**, 101, 2793.
- [26] B. M. Weckhuysen, I. E. Wachs, *J. Chem. Soc. Faraday Trans.* **1996**, 92, 1969.
- [27] J. E. Maslar, W. S. Hurst, W. J. Bowers, Jr, J. H. Hendricks, M. I. Aquino, I. Levin, *Appl. Surf. Sci.* **2001**, 180, 102.
- [28] N. F. Mott, *Trans. Faraday Soc.* **1947**, 43, 429.
- [29] N. Cabrera, N. F. Mott, *Rep. Prog. Phys.* **1949**, 12, 163.
- [30] R. N. Wenzel, *Ind. Eng. Chem.* **1936**, 28, 988.
- [31] A. B. D. Cassie, S. Baxter, *Trans. Faraday Soc.* **1944**, 40, 546.
- [32] M. Callies, Y. Chen, F. Marty, A. Pépin, D. Quéré, *Microelectr. Eng.* **2005**, 78–79, 100.
- [33] W. Lee, B. G. Park, D. H. Kim, D. J. Ahn, Y. Park, S. H. Lee, K. B. Lee, *Langmuir* **2009**, 26, 1412.
- [34] S. G. Mason, in *Wetting Spreading and Adhesion* (Ed.: J. F. Padday), Academic Press, New York and London **1978**, pp. 321–326.
- [35] R. G. Cox, *J. Fluid Mech.* **1983**, 131, 1.
- [36] P. G. de Gennes, *Rev. Mod. Phys.* **1985**, 57, 827.
- [37] R. Shuttleworth, G. L. J. Bailey, *Discuss. Faraday Soc.* **1948**, 3, 16.
- [38] J. F. Oliver, C. Huh, S. G. Mason, *J. Adhes.* **1976**, 8, 223.
- [39] R. J. Good, *J. Am. Chem. Soc.* **1952**, 74, 5041.
- [40] J. F. Oliver, C. Huh, S. G. Mason, *J. Colloid Interface Sci.* **1977**, 59, 568.